

EFFECT OF AGGREGATE SIZE ON ATTENUATION OF RAYLEIGH SURFACE WAVES IN CEMENT-BASED MATERIALS

By Laurence J. Jacobs,¹ Member, ASCE, and Joseph O. Owino²

ABSTRACT: This research uses laser ultrasonic techniques to study the effect of aggregate size on the attenuation of Rayleigh surface waves in cement-based materials. The random, multiphase, and heterogeneous nature of cement-based materials causes a high degree of material attenuation in the ultrasonic waves that propagate in these materials. Physically, these attenuation losses are due to a combination of absorption and the scattering losses due to material heterogeneity. Laser ultrasonics is an ideal methodology to measure attenuation in these materials because of its high fidelity, large frequency bandwidth, and absolute, noncontact nature. To investigate the effect of aggregate size on attenuation, this research uses a dual-probe, heterodyne interferometer to experimentally measure attenuation losses (as a function of frequency) in five different material systems (each with a different microstructure). These experimental results show that absorption, not scattering from the aggregate, is the dominant attenuation mechanism present in cement-based materials. As a result, aggregate size does not dominate attenuation.

INTRODUCTION

The successes of previous researchers (Papadakis 1965; Evans et al. 1978; Sannicé and Bilguty 1986) managed to relate the attributes of ultrasonic waves (such as attenuation) with specific microstructure parameters (such as grain size) in ceramic and metallic materials, but these relations have not occurred in cement-based materials. The primary problem with the ultrasonic interrogation of cement-based materials is their random, multiphase, and heterogeneous nature that causes complicated ultrasonic signals. The inherent difficulty in interpreting these signals is evidenced by the lack of quantitative knowledge about the propagation of ultrasonic waves in cement-based materials. As one example, there are no models that accurately explain the underlying mechanics of attenuation in these materials. This lack of comprehension has limited the development of quantitative ultrasonic techniques that are capable of characterizing cement-based materials. This research examines one fundamental question: What is the effect of aggregate size on attenuation?

As a brief review, attenuation of ultrasonic waves is due to two separate mechanisms: geometric and material attenuation. Geometric attenuation is an "extrinsic effect" that includes transducer aperture diffraction (where the finite dimensions of a transducer cause deviations from the ideal plane or spherical wave hypothesis) and specimen geometry (e.g., guided waves). For the ideal case of a point source and point detector in the far field, the amplitude of a Rayleigh surface wave, which propagates along a cylindrical wavefront, decreases as a function of the inverse square root of its propagation distance (Ewing et al. 1957). Material attenuation is an "intrinsic effect" caused by either absorption or scattering. Absorption losses are material effects such as viscoelastic behavior or the internal friction due to the work done at material interfaces when two materials are not elastically bonded. In contrast, scattering losses are due to material heterogeneity and are dependent upon the intrinsic length scale of the scatterer, number of scatterers per unit volume, distribution of scatterers, and acoustic

properties of scatterers in relation to the base material. An additional attenuation mechanism is possible if the scattering distorts the cylindrical (in this case) wavefront; this mechanism is driven by the scatterers but is different from scattering-based attenuation. Finally, nonlinear effects are possible; the generation of higher harmonics will cause (small) decreases in amplitude at the sonifying frequencies.

Material attenuation causes an exponential decrease in amplitude $e^{-\alpha r}$, where r is the propagation distance and α is the frequency-dependent (material) attenuation coefficient. Note that, because absorption and scattering losses are coupled, this attenuation coefficient α is the sum of both effects. Absorption increases linearly with frequency, whereas scattering is divided into three distinct regions depending upon the ratio of the mean scatterer diameter \bar{D} to the wavelength λ (Papadakis 1965). In the first region (Rayleigh regime), the mean diameter \bar{D} of the scatterers is very small when compared to the wavelength λ and the scattering coefficient is proportional to the fourth power of the frequency f

$$\alpha(f) = a_1 f + a_2 \bar{D}^3 f^4 \quad (1)$$

where a_1 = absorption coefficient; and a_2 = scattering coefficient. In the second region (stochastic regime), where the wavelength is approximately of the same order of magnitude as the mean scatterer diameter \bar{D} , the scattering coefficient varies with the square of the frequency

$$\alpha(f) = b_1 f + b_2 \bar{D} f^2 \quad (2)$$

where b_1 = absorption coefficient; and b_2 = scattering coefficient. In the third (diffusion regime), the wavelength is small in comparison to the mean scatterer diameter (note that this region will not be relevant to the ultrasonic wavelengths used in this research).

Owino and Jacobs (1999) developed a laser ultrasonic procedure to measure attenuation in cement-based materials. In brief, this procedure uses a multistation method to measure changes in Rayleigh surface wave amplitude (as a function of propagation distance and frequency) for signals that propagate through exactly the same material volume. This methodology uses a dual-probe interferometer to ensure that the laser source generates wave amplitudes that are truly constant. The second probe enables an independent, quantitative measure of each wave's amplitude and provides a normalization value that removes any variations in source strength.

The objective of the current study is to apply this laser ultrasonic procedure to experimentally examine the effect of aggregate size on the attenuation of Rayleigh surface waves in cement-based materials. This investigation relies on the high

¹Prof., School of Civ. and Envir. Engrg., Georgia Inst. of Technol., Atlanta, GA 30332-0355.

²Grad. Res. Asst., School of Civ. and Envir. Engrg., Georgia Inst. of Technol., Atlanta, GA.

Note. Associate Editor: Farhad Ansari. Discussion open until April 1, 2001. To extend the closing date one month, a written request must be filed with the ASCE Manager of Journals. The manuscript for this paper was submitted for review and possible publication on March 10, 2000. This paper is part of the *Journal of Engineering Mechanics*, Vol. 126, No. 11, November, 2000. ©ASCE, ISSN 0733-9399/00/0011-1124-1130/\$8.00 + \$.50 per page. Paper No. 22265.

fidelity, broadband, and noncontact nature of laser ultrasonics to measure attenuation in five different mortar specimens, each with a different microstructure. By using laser ultrasonic techniques, it is possible to experimentally generate and detect Rayleigh waves in cement-based materials without any of the frequency biases present in, for example, piezoelectric transducers. The noncontact nature of laser ultrasonics provides two additional advantages. First, there are no repeatability problems associated with coupling, an operation that can lead to losses that are even greater than the material attenuation. Second, the measurement process does not interfere with or influence the surface waves being monitored.

MICROSTRUCTURE OF MORTAR SPECIMENS

Cement-based materials typically consist of both coarse and fine aggregates held together by a binding matrix, usually portland cement. However, it is possible to make a less complicated (two-phase) cement-based material, mortar, by combining fine aggregates (sand) with a portland cement matrix. Mortar is a true cement-based material that contains critical microstructure characteristics such as material heterogeneity and mortar/aggregate interfaces. As a result, it is possible to use mortar to study attenuation losses in cement-based materials, without the added complication of coarse aggregate and an additional length scale.

Five mortar specimens are manufactured, each with the same water/cement and sand/cement ratios (0.4 and 2 by weight, respectively) but with different sizes of sand particles (fine aggregate). These five specimens provide five different material systems, each with a different microstructure. Each specimen is cast with sand particles that are generally of a single size (diameter). This “uniform distribution” mix design is in contrast to a typical cement-based material that normally contains a “well-graded distribution” of aggregate. As a result, all sand particles—the primary scatterers—in a single specimen have approximately the same length scale. The five specimens (material systems) are designated as follows: MS1 = no sand particles; MS2 = 0.25-mm sand particles; MS3 = 0.75-mm sand particles; MS4 = 1.5-mm sand particles; and MS5 = 3.5-mm sand particles. Note that all sand particles in a single material system are not exactly the same size. It is impossible

to have such a distribution in this natural material. However, all of the sand particles in a single material system are approximately the same size. These distributions are as uniform as possible for “real” sand. For example, consider MS4, with a designated length scale (sand size) of 1.5 mm. In this case 94% of the sand passes a No. 8 sieve (2.38 mm); 73% passes a No. 10 sieve (2 mm); 43% passes a No. 12 sieve (1.68 mm); 18% passes a No. 14 sieve (1.41 mm); and 7% passes a No. 16 sieve (1.19 mm). The sand distributions are similar for the other three material systems but centered on their respective length scales. Fig. 1 shows magnified digital images of typical areas for MS3 and MS5, enabling a qualitative, visual description of the considerable differences that exist between each of the material systems.

The specimens are cylinders, 125 mm in diameter and 75-mm thick, large enough so that reflections from the boundaries will not interfere with the waves of interest. The casting process consists of vacuuming and vibrating each specimen to ensure the removal of a majority of the entrapped air. This step is critical because it creates a specimen with a minimum amount of air voids. These air voids can potentially be the dominant length scale and thus overwhelm and mask the influence of the aggregate (sand particles). Finally, the specimens are covered with plastic sheeting, stripped at 2 days, immersed in a water bath for 26 days, air dried, saw cut (approximately 25 mm below the original top surface), and this surface is polished.

The acoustic impedances (longitudinal wave speed times mass density) of the portland cement matrix and sand particles are fairly close [9.8×10^6 kg/m²s for sand (quartz) and 8.9×10^6 kg/m²s for portland cement matrix], with <10% difference. However, cement-based materials also contain a significant interfacial zone between the matrix and aggregate—sand in this case—(Young et al. 1998) that complicates the attenuation process. As a result, a simple reflection/transmission model based on perfect interfaces does not provide a satisfactory representation of attenuation in these materials [see Jacobs and Whitcomb (1997) for details].

The microstructures of these five material systems are such that the length scale of the principal scatterers varies in size by an order of 10 (from 0.25 to 3.5 mm), plus MS1 contains no scatterers. It is important to note that these are “real” ce-

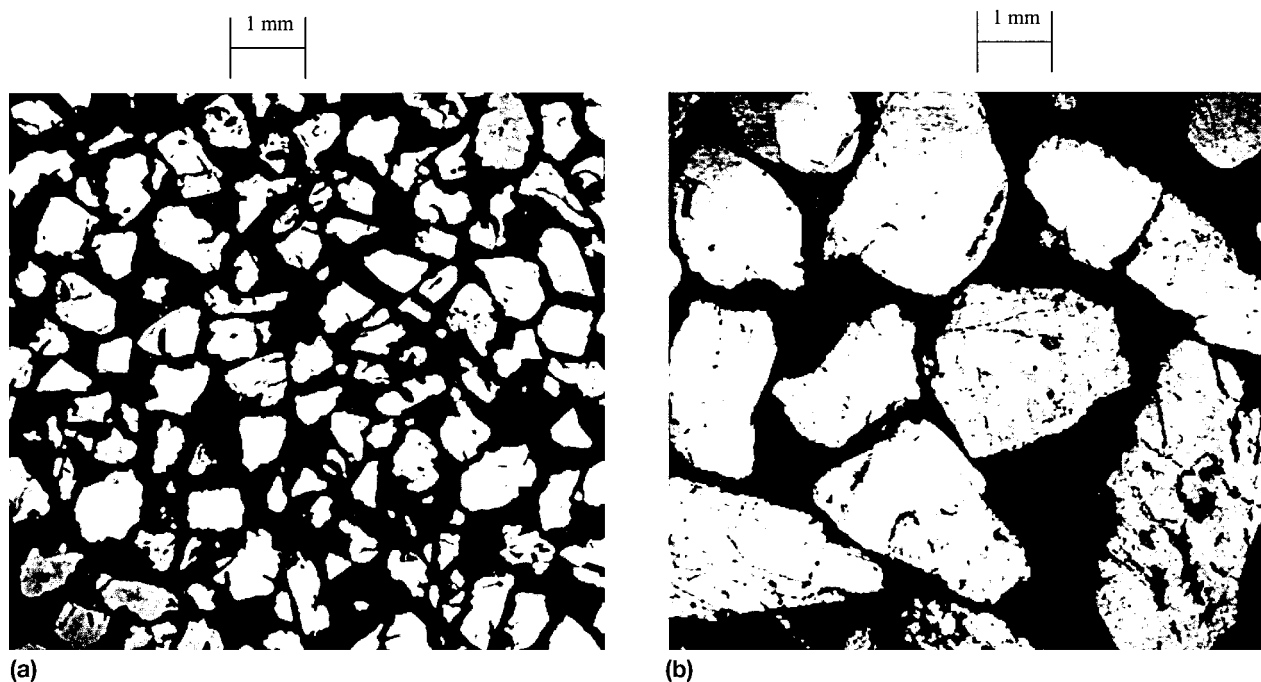


FIG. 1. Magnified Digital Images of Sand Particles: (a) MS3 = 0.75-mm Diameter; (b) MS5 = 3.5-mm Diameter

ment-based materials, so it is impossible to control the distribution of the aggregate, either within the same specimen or from specimen to specimen. In addition, there are other microstructure issues such as the high level of variability and randomness in the material and existence of voids and air bubbles. As a result, the proposed experimental procedure uses an averaging technique described in the next section to measure attenuation for each material system.

The parameter examined in this study is the length scale of the scatterer (aggregate) relative to the interrogating wavelength. The Rayleigh surface wave speed in mortar (measured in this study) is about 2,400 m/s, so the wavelengths of some typical Rayleigh surface waves include: frequency f of 100 kHz, wavelength λ is 24 mm; f of 500 kHz, λ is 4.8 mm; f of 1 MHz, λ is 2.4 mm; and f of 5 MHz, λ is 0.48 mm. In light of the microstructure of specimens MS1–MS5, it is clear that Rayleigh surface waves with a frequency range up to 5 MHz provide a wide range of ratios between potential scatterers and wavelengths.

EXPERIMENTAL PROCEDURE

Rayleigh surface waves are generated with the pulse of a Q-switched Nd:YAG laser using an ablation generation mechanism that creates repeatable, broadband ultrasonic waveforms in mortar. The Nd:YAG laser (1,064 nm) used in this study emits a 450 mJ, 4–6 ns pulse. The beam that strikes the specimen is attenuated and focused to a spot size of 0.5 mm; the energy striking the mortar surface is on the order of 10 mJ. Laser detection of these Rayleigh surface waves is accomplished with a dual-probe heterodyne interferometer that is a modified version of the instrument described in detail in Bruttomesso et al. (1993). This optical device uses the Doppler shift to simultaneously measure out-of-plane surface velocity (particle velocity) at two points (0.5-mm spot size) on the specimen's surface. The interferometer, which works by measuring frequency changes in the light reflected off the specimen's surface, makes high fidelity, absolute measurements of surface velocity over a bandwidth of 100 kHz to 10 MHz.

It is important to note that all specimens examined in this research have polished surfaces. This preparation enables true noncontact detection (there are no artificial surface treatments such as reflective tape) as well as provides a consistent surface for Rayleigh wave propagation. In addition, each signal is low-pass filtered at 10 MHz and represents an average of up to 200 shots. This averaging increases the signal-to-noise ratio (SNR) by the square root of N , where N is the number of averages.

The attenuation of Rayleigh surface waves is measured with a multistation method in which the source is fixed, one receiver (the normalization probe) remains at a fixed distance d from the source, and the second receiver is located at a variable distance r from the source [see Owino and Jacobs (1999) for details]. A Rayleigh surface wave is generated and detected in this position, then probe No. 2 is moved a prescribed distance (with a micrometer) away from the source (along a line on the surface of the specimen), and the procedure is repeated. Note that, although the position of probe No. 2 changes, the locations of both the source and the normalization probe remain the same. As a result, the signals measured by the normalization probe ensure that each waveform detected by probe No. 2 is due to exactly the same source.

This study averages 56 separate waveforms to determine the attenuation coefficient for each material system. Specifically, seven different random lines along the specimen's polished surface are interrogated with the multistation method. Eight different waveforms, measured with probe No. 2 and with propagation distances r that vary from (approximately) 20 to 60 mm, are collected along each line. The frequency-depen-

dent attenuation coefficient α is calculated by first normalizing each geometrically corrected frequency spectrum (the eight signals measured with probe No. 2) to that of a reference spectrum (the waveform from its normalization probe). This normalization is accomplished with a point-by-point division in the frequency domain. The final step is to perform a linear regression at each discrete frequency (using the results from all 56 normalized signals) on a semilogarithmic plot, thus modeling the exponential character of α (Owino and Jacobs 1999).

It is important to note that there are variations in the signals measured along different lines (even within the same material system) that necessitate the large number of averages in the proposed scheme. This variation is a direct result of the high level of variability and randomness in cement-based materials, including the distribution of the aggregate and existence of voids. A benefit of the proposed averaging procedure is the removal of any small variations due to source location; each waveform measured with probe No. 2 is normalized with its corresponding source signal (normalization probe). An ultrasonic signal created by a laser source is directly dependent upon the "spot" (volume) of material illuminated by the laser. Unfortunately, in a heterogeneous material such as mortar, a different spot of material is illuminated every time the source is moved. However, the multistation method keeps the laser source in exactly the same location for each line (each of the eight signals is created by exactly the same source), so averaging with the normalization probe signal allows for the combination of signals from all lines to calculate an average attenuation for each material system.

EXPERIMENTAL RESULTS FOR MS3

As a detailed demonstration of the proposed procedure, consider the results for material system MS3. Fig. 2(a) shows time domain signals for eight different propagation distances (created by the same source) along a typical line in MS3. Overall, the shape of the Rayleigh surface waves becomes broader as the propagation distance r increases from 19.6 mm (closest) to 49.5 mm (farthest). The Rayleigh surface wave portion of each of these signals is windowed (a 2.5- μ s window that represents 375 points in this instance), padded to its original length (15,000 points), corrected for geometric spreading (multiplied by the square root of its propagation distance), and transformed into the frequency domain with a fast Fourier transform (FFT). Fig. 2(b) shows the corresponding frequency domain spectrum (magnitude) for each of the eight propagation distances. Notice that the corrected Rayleigh surface wave amplitudes in Fig. 2(b) are generally larger the closer the source is to the receiving probe, a qualitative indication of the high degree of material attenuation present in cement-based materials. In addition, note the wide frequency bandwidth represented by these spectra (DC to > 2 MHz), although most of the signal (amplitude) is < 1.5 MHz. A closer examination of the frequency domain plots shows that the center frequency shifts to the left (decreases) the farther the propagation distance, showing that the original, high frequency portion of the signal is essentially lost as a Rayleigh surface wave propagates away from its source. Furthermore, the spectra are very similar up to a minimum frequency (on the order of 300 kHz) and then begin to diverge from each other.

Note that the correction for geometric spreading assumes a cylindrical wavefront. This is only true if wavefront distortion due to scatterers is not a factor and measurements are made in the far field. The point source/receiver nature of laser ultrasonics and long propagation distances, relative to wavelength, enable far field measurements. For example, a test case, which uses the same measurement procedure, in an aluminum sample shows that it is possible to measure Rayleigh surface wave

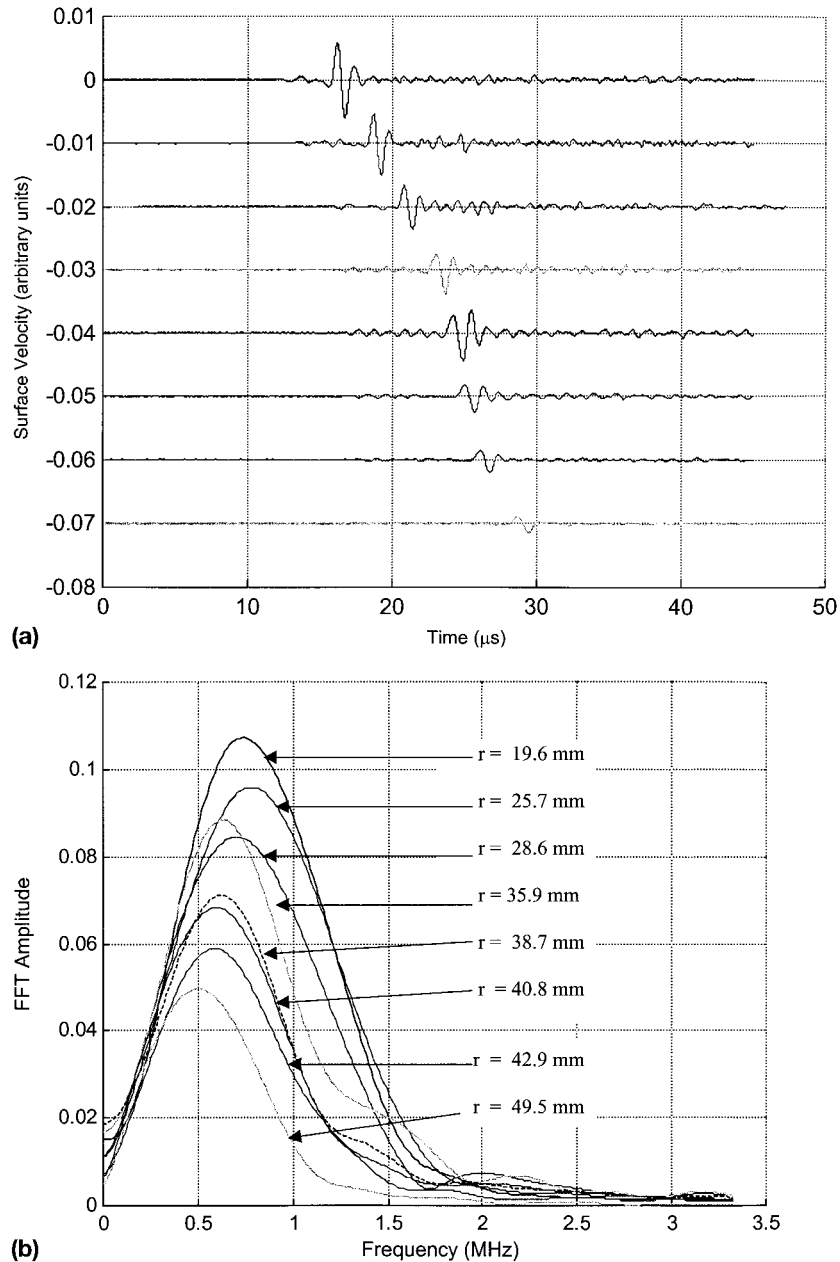


FIG. 2. Comparisons of: (a) Eight Time Domain Signals (Created by Same Source) in MS3 (Propagation Distances r from Top-to-Bottom = 19.6, 25.7, 28.6, 35.9, 38.7, 40.8, 42.9, and 49.5 mm); (b) Magnitudes of Frequency Domain of Rayleigh Wave Portion (Corrected for Geometric Spreading) of Eight Signals Shown in Fig. 2(a)

attenuation without correcting for beam field diffraction (Owino and Jacobs 1999). This avoidance of aperture diffraction effects with laser techniques also is reported by Pouet and Rasolofosaon (1993). The proposed procedure does not provide an independent measure of wavefront distortion due to scattering; this check, which requires multiple, full field measurements, is beyond the scope of this work. Note that, because this procedure windows and isolates the Rayleigh surface wave portion of each signal, these attenuation coefficients should include any attenuation due to wavefront distortion.

Six other lines are interrogated, and the 56 normalized signals are used to calculate the material attenuation coefficient α . Fig. 3(a) shows that the resulting attenuation coefficient α is essentially linearly increasing through a wide frequency range (with a bandwidth from 200 kHz to 1.1 MHz), followed by a region of decrease and an essentially random pattern.

Consider these attenuation results in terms of coherence. Coherence is defined as the fractional portion of the output signal (the measured Rayleigh surface wave in this case) that

is due to the input signal (the laser source in this case) at a specific frequency f (Owino and Jacobs 1999). Coherence is especially helpful in determining the frequency bandwidth through which an experimentally measured attenuation coefficient α is reliable. A coherence value of 1 indicates perfect coherence between the input and output signals (100% of the output is due to the input), while a coherence of <1 indicates either excessive noise or a nonlinear response at a specific frequency. Frequency components whose coherence values are <0.9 are usually rejected. Following a procedure described in Owino and Jacobs (1999), coherence values are calculated for the same seven lines and are averaged. Fig. 3(b) shows the coherence (plotted as a function of frequency) for MS3. Note that the cutoff frequency (the maximum linear range) of 1.1 MHz compares very well with the point at which the coherence value becomes <0.9 , indicating "low" coherence. The same low coherence exists for frequencies <200 kHz. As a result, all attenuation values <200 kHz and >1.1 MHz are rejected. By examining the frequency domain plots in Fig. 2(b),

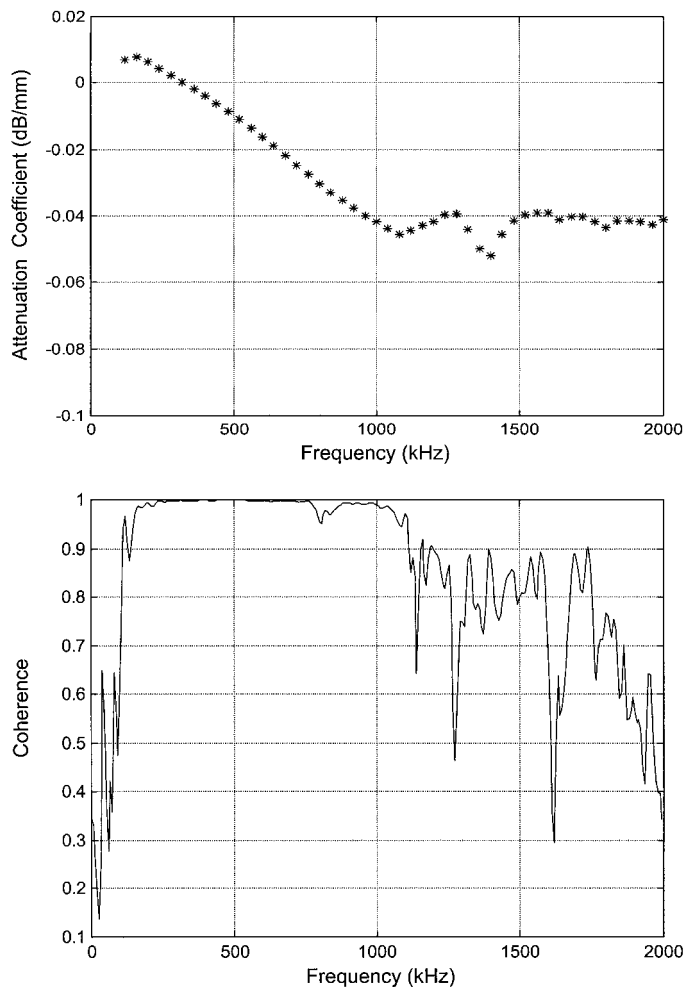


FIG. 3. Plots versus Frequency for MS3: (a) Attenuation Coefficient α ; (b) Coherence

it is clear that the low coherence in the frequency range >1.1 MHz is due to low SNR in this frequency range, not non-linearity. However, this low SNR is a material property, not a manifestation of the measurement system. For example, using this same laser ultrasonics system, attenuation measurements are made in aluminum for frequencies as high as 5 MHz.

Note that the attenuation coefficient [in Fig. 3(a)] does not pass through the origin (zero attenuation for zero frequency); in fact, attenuation values become positive <300 kHz. This spurious behavior is due to the small level of attenuation present at these low frequencies—witness the similarity in frequency spectra (for all propagation distances) <300 kHz in Fig. 2(b). As a result, random noise can dominate this portion of the multistation attenuation calculations, resulting in imprecise values. The calculation of attenuation in this low frequency range is not of primary concern for the aggregate sizes considered in this study, and the poor attenuation behavior is aggravated by the small propagation distances (in relationship to the long wavelengths) for these low frequencies.

To determine the contributions of absorption and scattering, consider these attenuation results in terms of the material attenuation models for the Rayleigh and stochastic scattering regimes described by (1) and (2). The behavior of the attenuation curve in the region of good coherence is essentially linear. It is senseless to fit a function containing only a single fourth- or second-order term. First, ignore the effect of scattering and assume only a linear relationship between frequency and attenuation. Next, assume that both absorption and Rayleigh scattering are present and fit a polynomial that has both a linear and fourth-order term. Finally, assume that both ab-

sorption and stochastic scattering are present and fit a polynomial that has both a linear and second-order term. The results of this regression analysis yield the following equations:

$$\alpha = 1.96 \times 10^{-2} - 6.08 \times 10^{-5}f \quad (3a)$$

$$\alpha = 1.88 \times 10^{-2} - 5.844 \times 10^{-5}f - 2.23 \times 10^{-15}f^4 \quad (3b)$$

$$\alpha = 1.81 \times 10^{-2} - 5.41 \times 10^{-5}f - 6.519 \times 10^{-9}f^2 \quad (3c)$$

The functions described by (3) are all essentially linear; the plots of each of these functions are visually indistinguishable from each other, each representing effectively a linear fit to the discrete attenuation data of Fig. 3(a). Note that the absorption coefficients of f in (3a) and (3b) are very close (4% difference), indicating that the attenuation mechanism in these cement-based materials is dominated by absorption, whereas the scattering effects are negligible in comparison. The stochastic regime model of (3c) yields the same results; scattering is negligible and absorption dominates. In view of these results, the scattering contribution is considered to be insignificant in comparison with the absorption losses present and a linear (absorption coefficient only) attenuation model is adopted. This linear model provides a simple, but accurate, tool that enables a quantifiable comparison of material attenuation for the five different material systems.

EXPERIMENTAL RESULTS FOR EACH MATERIAL SYSTEM

Fig. 4(a) shows typical Rayleigh surface waves obtained for each of the five material systems. Each Rayleigh surface wave has propagated the same distance (19.5 mm). It is again important to note that the source that produces each of these waveforms is not exactly the same, also a direct comparison of wave amplitudes is problematic. Fig. 4(a) qualitatively shows that there are small differences in waveform shape for each material system, but overall they are very similar. The corresponding frequency domain plots (magnitudes) for the Rayleigh surface wave portions of the signals in Fig. 4(a) are depicted in Fig. 4(b). To make a fair comparison, each frequency plot in Fig. 4(b) is normalized to its largest amplitude. Fig. 4(b) shows small frequency shifts, but these frequency shifts do not follow any trend from material system to material system and cannot be related to aggregate size. In addition, the maximum frequency that propagates in each material system is effectively the same (approximately 2 MHz). Figs. 4(a and b) do not illustrate any consistent or definitive relationships between Rayleigh surface wave properties (time or frequency domain) and the microstructure of each material system; in fact, the similarities between these signals in the time and frequency domains are much greater than the differences. This degree of similitude is unexpected, especially when considering that there is an order of magnitude difference in aggregate size and that MS1 has no aggregate.

The procedure described in the previous section is used to measure average, frequency-dependent attenuation coefficients α , together with their corresponding coherence values, for all five material systems. These results show the same trends exhibited in MS3 (and presented in Fig. 3); the linearity of the attenuation coefficients disappears at approximately the same frequency where coherence indicates unreliable values (coherence <0.9). Fig. 5(a) shows the reliable portions of the attenuation coefficients for each of the material systems.

Although each material system has almost the same lower frequency limit (200 kHz), the upper cutoff frequencies (upper frequency limit of reliable attenuation indicated by coherence) are different. However, these cutoff frequencies do not necessarily follow a specific pattern that can be related to features in their respective microstructures, such as aggregate size. For

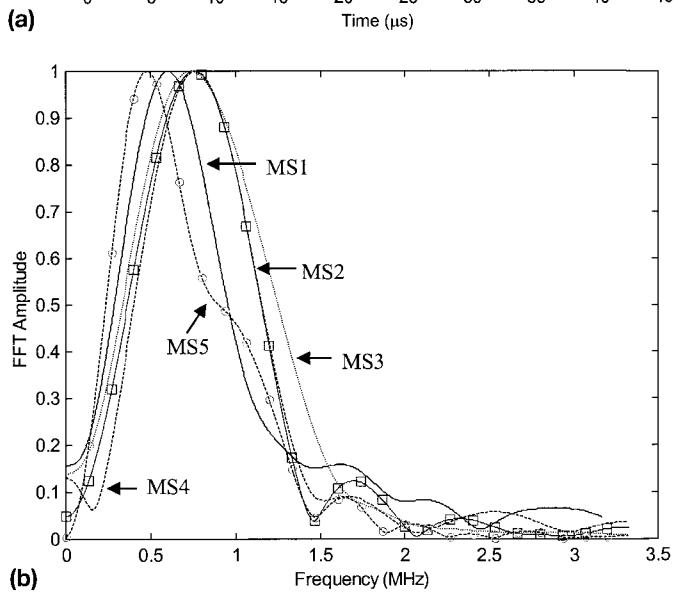
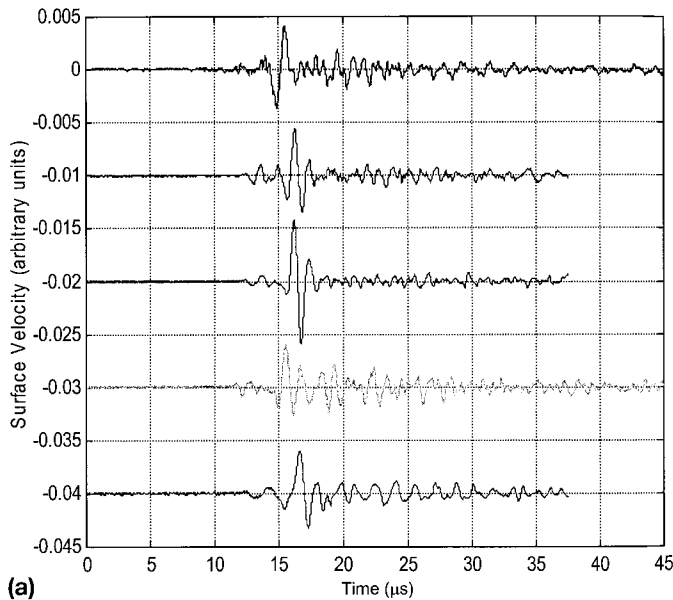


FIG. 4. Comparisons of: (a) Typical Time Domain Signals for MS1–MS5 (Top-to-Bottom, Respectively) for Same Propagation Distance ($r = 19.5$ mm); (b) Magnitudes of Frequency Domain of Normalized Rayleigh Wave Portion of Five Signals Shown in Fig. 4(a)

example, cutoff frequency does not decrease with increasing scatterer size. This demonstrates that the size of the scatterers (aggregate) is not the dominant feature in predicting attenuation in cement-based materials. Note that scattering losses depend upon several factors (besides scatterer size), such as the number of scatterers per unit volume, distribution of scatterers, and acoustic properties of scatterers in relation to the base material. This study only varies aggregate size, an easily controllable factor in real cement-based materials.

Five first-order polynomials (straight lines) are fit to the data shown in Fig. 5(a) to determine the relationship between attenuation (absorption coefficient) and frequency for each material system

$$\alpha_1 = 5.27 \times 10^{-2} - 1.42 \times 10^{-4}f \quad (4a)$$

$$\alpha_2 = 5.17 \times 10^{-2} - 1.88 \times 10^{-4}f \quad (4b)$$

$$\alpha_3 = 1.96 \times 10^{-2} - 0.608 \times 10^{-4}f \quad (4c)$$

$$\alpha_4 = -8.85 \times 10^{-2} - 1.09 \times 10^{-4}f \quad (4d)$$

$$\alpha_5 = 5.46 \times 10^{-2} - 1.95 \times 10^{-4}f \quad (4e)$$

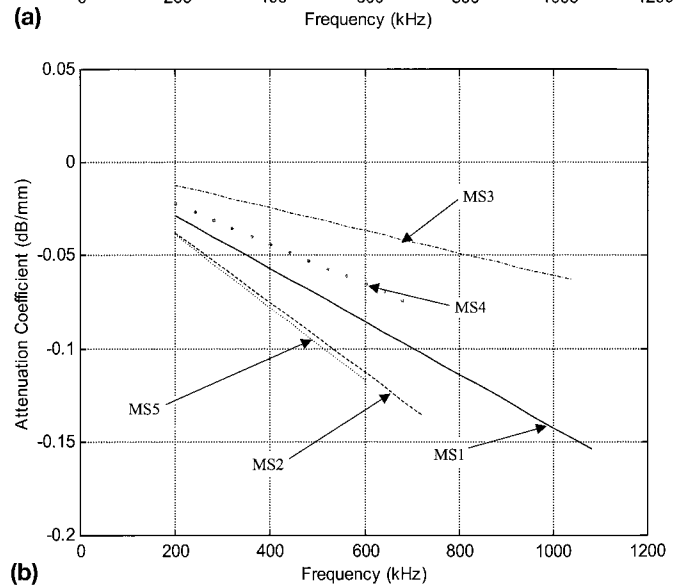
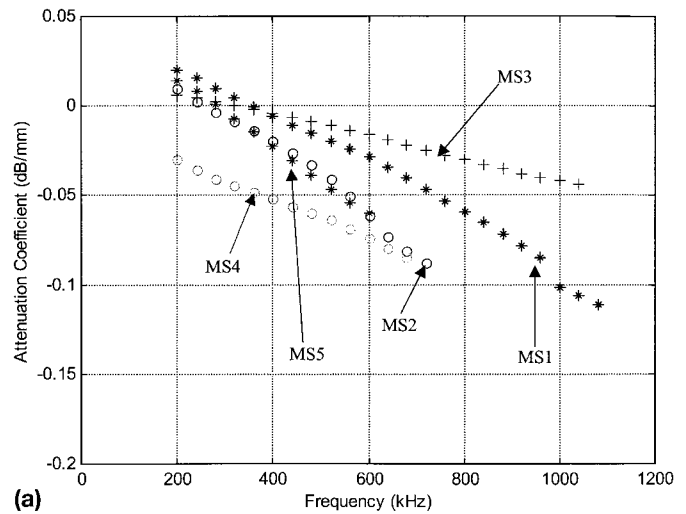


FIG. 5. Plots of Attenuation Coefficients α versus Frequency for MS1–MS5: (a) Reliable (Based on Coherence) Portions; (b) Absorption Only (Linear) Model

The absorption coefficients of f in (4) quantify the absorption losses present in material systems MS1–MS5, respectively. The absorption coefficients (slopes) shown in (4) are presented in Fig. 5(b) but are shifted (to enable a visual comparison) so that, at zero frequency, the attenuation value is also zero (zero y -intercept). The absorption coefficients in Fig. 5(b) do not follow a pattern that can be related to aggregate size.

One potential source of absorption losses in cement-based materials is friction that occurs in the interfacial zone between the aggregate and matrix. These absorption losses are indirectly related to scatterer size and distribution. One possible manifestation of this connection could be decreasing absorption coefficients (slope of the attenuation coefficient) for increasing scatterer size, but this relationship is not evident in Fig. 5(b). However, all of the slopes (absorption losses) are in the same range regardless of microstructure, indicating that absorption attenuation is not dominated by aggregate size. As a result, it should be possible to develop generic measures of absorption attenuation (and thus material attenuation) in cement-based materials that are independent of microstructure.

CONCLUSIONS

This research demonstrates the effectiveness of using laser ultrasonic techniques to study the effect of aggregate size on attenuation losses in cement-based materials. It is possible to

experimentally measure the frequency-dependent material attenuation coefficient α over a broad frequency bandwidth in a variety of material systems. These experimental measurements are only possible because of the high fidelity, (frequency) unbiased, broadband, point source/point receiver, and noncontact nature of laser ultrasonics.

It is observed that, even within a given material system, there is a considerable variability in attenuation. This variation is attributed to the randomness and variability present in cement-based materials and is a primary reason for the limited amount of research in this area. However, this work develops an average attenuation for the entire material system that is an excellent representation of the frequency-dependent attenuation coefficient for a particular microstructure. The predominate attenuation feature observed in these experiments is that scattering losses are negligible when compared to the absorption losses present. As a result, aggregate size does not dominate attenuation. In addition, the maximum linear value of frequency cannot be related to the maximum scatterer length. Finally, because all of the absorption losses are on the same order, it is extremely difficult to relate these attenuation losses to the microstructure of the specific cement-based material being interrogated.

APPENDIX. REFERENCES

- Bruttomesso, D. A., Jacobs, L. J., and Costley, R. D. (1993). "Development of an interferometer for acoustic emission testing." *J. Engrg. Mech.*, ASCE, 119(11), 2303–2316.
- Evans, A. G., Tittmann, B. R., Ahlberg, L., Khuri-Yakub, B. T., and Kino, G. S. (1978). "Ultrasonic attenuation in ceramics." *J. Appl. Phys.*, 49, 2669–2679.
- Ewing, M., Jardetzky, W., and Press, F. (1957). *Elastic waves in layered media*, McGraw-Hill, New York.
- Jacobs, L. J., and Whitcomb, R. (1997). "Laser generation and detection of ultrasound in concrete." *J. Nondestructive Evaluation*, 16, 57–65.
- Owino, J. O., and Jacobs, L. J. (1999). "Attenuation measurements in cement-based materials using laser ultrasonics." *J. Engrg. Mech.*, ASCE, 125(6), 637–647.
- Papadakis, E. P. (1965). "Ultrasonic attenuation caused by scattering in polycrystalline metals." *J. Acoustical Soc. of Am.*, 37, 711–717.
- Pouet, B. F., and Rasolofosaon, N. J. P. (1993). "Measurement of broadband intrinsic ultrasonic attenuation and dispersion in solids with laser ultrasonics." *J. Acoust. Soc. Am.*, 93, 1286–1292.
- Sanniee, J., and Bilguty, N. M. (1986). "Quantitative grain size evaluation using ultrasonic backscattered echoes." *J. Acoust. Soc. Am.*, 80, 175–184.
- Young, J. F., Mindess, S., Gray, R. J., and Bentur, A. (1998). *The science and technology of civil engineering materials*, Prentice-Hall, New York.